A&A 522, A2 (2010)
DOI: 10.1051/0004-6361/200913292

Astronomy & Astrophysics

Searching for the sub-stellar companions in the LkCa15 proto-planetary disk

M. Bonavita[1,2], G. Chauvin[3], A. Boccaletti[4], V. Pietu[5], P. Baudoz[4], J. L. Beuzit[3], A. Dutrey[7], S. Guilloteau[7], A. M. Lagrange[3], D. Mouillet[3], and G. Niccolini[6]

[1] INAF-Osservatorio Astronomico di Padova, Vicolo dell'Osservatorio 5, 35122 Padova, Italy
e-mail: mariangela.bonavita@oapd.inaf.it
[2] Dipartimento di Astronomia, Universitá degli Studi di Padova, Vicolo dell'Osservatorio 2, 35122 Padova, Italy
[3] Laboratoire d'Astrophysique, Observatoire de Grenoble, UJF, CNRS, rue de la piscine, 38400 Saint-Martin d'Hères, France
[4] LESIA, Observatoire de Paris Meudon, 5 pl. J. Janssen, 92195 Meudon, France
[5] Institut de Radio-Astronomie Millimétrique, 300 rue de la Piscine, Domaine Universitaire, 38406 Saint-Martin d'Hères, France
[6] Lab. H. Fizeau, CNRS UMR 6525, Univ. de Nice-Sophia Antipolis, Observatoire de la Côte d'Azur, 06108 Nice Cedex 2, France
[7] Laboratoire d'Astrophysique de Bordeaux (LAB), Université Bordeaux 1, Bordeaux, France; CNRS/INSU-UMR 5804, BP 89, 33270 Floirac, France

Received 14 September 2009 / Accepted 20 April 2010

ABSTRACT

Context. Recent sub-millimetric observations at the Plateau de Bure interferometer showed a cavity of ~46 AU in radius in the proto-planetary disk of the T Tauri star LkCa15 (V1079 Tau), located in the Taurus molecular cloud. Additional Spitzer observations have corroborated this result which can possibly be explained by a massive ($\geq 5 M_{\rm Jup}$) planetary companion, a brown dwarf or a low-mass star companion at about 30 AU from the star.

Aims. We used the most recent developments of high angular resolution and high-contrast imaging to directly search for this putative companion, and to bring new constraints on its physical and orbital properties.

Methods. The NACO adaptive optics instrument at the VLT was used to observe LkCa15 with a four-quadrant phase-mask coronagraph to access small angular separations at relatively high contrast. A reference star at the same parallactic angle was carefully observed to optimize the quasi-static speckles subtraction (limiting our sensitivity by less than 1.0″).

Results. Although we do not report any positive detection of a faint companion that would be responsible for the observed gap in LkCa15's disk (25−30 AU), our detection limits start constraining its probable mass, semi-major axis and eccentricity. Using evolutionary model predictions, the Monte Carlo simulations exclude the presence of low eccentric companions with masses $M \geq 6\ M_{\rm Jup}$ and orbiting at $a \geq 100$ AU with a significant level of confidence. For closer orbits, brown dwarf companions can be rejected with a detection probability of 90% down to 80 AU (at 80% down to 60 AU). Our detection limits do not permit us to access the star environment close enough to fully exclude the presence of a brown dwarf or a massive planet within the disk's inner activity (i.e. at less than 30 AU). Only, further and higher contrast observations should unveil the existence of this putative companion inside the LkCa15 disk.

Key words. stars: pre-main sequence – protoplanetary disks – instrumentation: adaptive optics

1. Introduction

The first glimpses of the planetary formation were caught more than two decades ago (Smith & Terrile 1984). After the discovery of the first extrasolar planet around a solar-type star (51 Peg, see Mayor & Queloz 1995), more than 400 planets have been found, mainly using the radial velocity technique (RV). However, the explored time span limits the radial velocity study (as well as pulsar timing, micro-lensing, photometric transit, astrometric techniques) to the close (≤4−5 AU) circumstellar environment. To understand the way exo-planetary systems form and evolve at wider orbits, it is consequently particularly interesting to use a complementary technique, such as direct imaging.

Around young solar analogues the current deep imaging performances permit the detection of companions down to the brown dwarf (BD) and planetary mass regimes. Typical separations larger than 50−100 mas (i.e. ≥5−10 AU for a star at 100 pc) can be explored for BD companions, and for planetary mass objects typical separations in the range 200−400 mas (i.e. ≥20−40 AU for a star at 100 pc).

The high-contrast and high angular resolution imaging capabilities of current instruments are also confirmed by the discoveries of other planetary mass companions. The discoveries of the planetary mass companions like 2M1207 b (Chauvin et al. 2004) and, more recently around Fomalhaut (Kalas et al. 2008), a triple system around HR 8799 (Marois et al. 2009) and a close candidate around β Pic (Lagrange et al. 2009). To resolve ultra-cool and light companions, large telescopes equipped with adaptive optics (AO) are required, as well as dedicated focal devices, such as coronagraph and differential imagers.

Of special interest is the detection of planets that are still embedded in their parental proto-planetary disk, as this may give us clues about the timescales for planet formation and about the disk dissipation mechanisms. Indirect information can be obtained from gaps and asymmetries observed in the disk structures detected through scattered light images in near infrared (NIR) (e.g. for HD 141569, see Augereau et al. 1999) or through

millimeter interferometric measurements, like the ones recently done for AB Aur (Piétu et al. 2005) and TW Hydra (Hughes et al. 2007). Two controversial discoveries have been recently obtained, one with RV for the giant planet ($M \sim 10\ M_{\rm Jup}$) at 0.04 AU in the disk that surrounds TW Hya (Setiawan et al. 2008; Huélamo et al. 2008), the other by differential polarimetric and coronagraphic imaging for a point source (that can be explained by the presence of a companion or by an over-density in the disk due to dust accretion on an unseen companion) in the outer annulus of dust of the AB Aur disk (Oppenheimer et al. 2008). More recently, a planetary candidate has been detected in the β Pic circumstellar disk (Lagrange et al. 2009). If confirmed, these companions will be a direct evidence for the link between planetary formation and the main morphological and dynamical peculiarities of transition disks.

We present the results of NACO observations, taken with a four-quadrant phase-mask coronagraph, which aims at offering enhanced detection performances at small angular separations. Our goal was to detect the companion responsible for the large gap observed at mm wavelengths in the disk that surrounds the young star LkCa 15 (see Piétu et al. 2006).

After summarizing the properties of this star and its proto-planetary disk in Sect. 2, we present the NACO observations and the data reduction and analysis in Sect. 3 and 4 respectively. We finally report our detection limits in Sect. 5 and discuss them with regards to the domain of mass and orbital parameters explored for a putative companion.

2. LkCa 15

The source LkCa 15 (V1079 Tau: $V = 12.09$, $K = 8.16$, K5 and $d \sim 140$ pc) is a T Tauri star with an age of ~3−5 Myr (see Simon et al. 2000; Bertout & Genova 2006), located in a hole of the Taurus molecular cloud. Piétu et al. (2006) led sub-mm observations of the proto-planetary disk of LkCa 15, using the Plateau de Bure interferometer with an angular resolution of about 0.4″. The observations were made in "track-sharing", to observe LkCa 15 and the Herbig star MWC 480 with a common calibration curve. Any morphological difference between the two targets is thus genuine. They found a clear inner hole around LkCa 15 while MWC 480 is centrally peaked. This was confirmed by the data modeling, with a derived inner hole of ~46 AU (i.e. the size of our own solar system). A multi-isotope analysis of the CO rotational lines led Piétu et al. (2007) to derive the physical properties of the outer circumstellar disk surrounding the star. Contrary to the other system studied in a similar way, no clear vertical temperature gradient was found in the disk structure, possibly due to the peculiar geometry of LkCa 15 disk.

Piétu et al. (2006) discussed the possible mechanisms that could explain the inner hole structure (which is not completely empty, because some IR excess is present above the stellar black body. See Bergin et al. 2004). Planetary formation or a low-mass companion seem to be plausible explanations because the LkCa15 disk is quite massive. Indeed Simon et al. (2000) estimated from the kinematics a total mass for the system of $M_{\rm dyn} = 1.00 \pm 0.1\ M_{\odot}$. This is the maximal mass of the putative companion to 0.2 $M_{\odot}$, since the mass of LkCa 15 could hardly be less than 0.8 $M_{\odot}$, due to its spectral type. This value agrees with a recent estimate of the mass of the star obtained by Bertout et al. (2007). Using a new distance estimate by Bertout & Genova (2006), they confirmed LkCa 15 as a kinematic member of the Taurus association seen through a hole in the molecular cloud, retrieving a mass value of $1.12 \pm 0.08\ M_{\odot}$.

Additional results obtained by Alexander et al. (2006) also suggest that other mechanisms such as photo-evaporation are unlikely to be effective due to the high disk density, which is significantly higher than what would be expected if the photo-evaporation were to start propagating beyond 20−30 AU. Piétu et al. (2006) suggest that a ~5−10 $M_{\rm Jup}$ planet orbiting at 30 AU would be sufficient to evacuate the inner 50 AU of the LkCa 15 disk. Similar conclusions were reached by Espaillat et al. (2007) with Spitzer observations and the modeling of the SED of LkCa 15. Their analysis suggests that a gap is present in the disk of LkCa 15, with an inner disk going from 0.12−0.15 AU to 4−5 AU, and an outer disk with an inner radius 46 AU, which perfectly agrees with the findings of Piétu et al. (2006). They also concluded that planetary formation or a close-in stellar or sub-stellar companion are the most probable explanations for the circumstellar material shape around LkCa15.

3. Observations

3.1. Telescope and instrument

The observations were performed on 2007 December 26 at ESO/Paranal, using NACO, the AO-assisted near-IR camera NAOS-CONICA (Rousset et al. 2003) mounted on one of the Nasmyth focus of the UT4 8m-telescope. Among the numerous NACO observing modes (Lenzen et al. 2003), the classical and coronagraphic imaging modes were used.

Coronagraphic observations were performed with the four-quadrant phase mask (4QPM) optimized for $K_{\rm s}$ band observations. The S13 objective (FoV of 14″ × 14″ and plate-scale of 13.25 mas/pixel) was chosen for a more precise centering with the 4QPM and a better sampling of the point spread function (PSF). The 4QPM splits the focal plane into four equal areas, two of which are phase-shifted by π. As a consequence, a destructive interference occurs in the relayed pupil and the on-axis starlight rejected on the edge of the geometric pupil is filtered with a Lyot-stop, which is a circular hole 90% of the pupil size. The advantage over the classical Lyot mask is the possibility to access inner angular separations lower than 0.35″ (the smallest NACO occulting mask) at a relatively high contrast (see Boccaletti et al. 2004, 2008).

However, a significant part of the starlight is left in the focal plane due to uncorrected aberrations composed of a dynamical halo averaging over time plus a quasi-static halo corresponding to optical aberrations along the optical train (from telescope to detector). To mitigate this problem, a coronagraphic image of a reference star was taken just after our science target observations with the same instrumental settings to serve for speckle calibration in an image-subtraction process. This reference star (BD + 22 729, $V = 11.5$, $K = 7.9$) has similar visible and NIR-magnitudes to ensure a similar AO correction and signal-to-noise at the detector. Moreover, observations were performed to match the parallactic angle with LkCa15, i.e the instrumental pupil configuration, to optimize the overlap of the speckle pattern and the diffraction spikes position in the final subtracted image of LkCa15.

3.2. Observing strategy

The coronagraphic observations were preceded by a classical imaging sequence that provides a photometric reference. A neutral density (1.12% transmission) and narrow band filters at 2.17 μm were used to serve as an image-quality check and as photometric reference for the coronagraphic observations.

Table 1. Observing parameters used for each source, observed in classical and coronagraphic imaging.

Object	LkCa15 (Classical)	LkCa 15 (Coronagr.)	BD +22 729 (Coronagr.)
Filter	ND + $NB_{2.17}$	K_s	K_s
Objective	S13	S13	S13
t_{int} (s)	30	24	24
$N_{frame} \times N_{exp}$	2×1	4×8	4×8
t_{int}[sky] (s)	30	24	24
$N_{frame} \times N_{exp}$[sky]	2×1	4×1	4×1

Notes. The individual integration time (t_{int}), the number of frames (N_{frame}) averaged by the detector and the number of repeated exposures (N_{exp}) are reported on source and on sky. At the end, $N_{frame} \times N_{exp}$ gives the number of images available for the data reduction and analysis.

Table 1 summarizes the observing parameters. During the coronagraphic observing sequence, the precise centering of the science target behind the focal plane mask was critical to maximize the central star attenuation. The coronagraphic observations were acquired at two instrument positions rotated by 33°. Sky images were immediately observed for LkCa15 and its reference after each coronagraphic sequence.

4. Data reduction and analysis

4.1. Image processing and selection

The data were processed using the Eclipse[1] reduction software (Devillard 1997) for bad pixel correction, flat fielding and sky subtraction. Individual frames were inspected by eye to remove all low-quality images degraded by waffle aberrations or variable AO corrections. Finally, only LkCa15 and BD + 22 729 images with similar parallactic angles were selected to optimize our PSF-subtraction. Among the initial data set of eight images per source and per rotator position, only three were kept after the selection process totaling an integration time of 288 seconds.

4.2. Subtraction of the diffraction residuals

The purpose is to properly subtract the stellar contribution from the LkCa15 images. For each rotator and parallactic angle position, the reference star was shifted at a 0.1-pixel accuracy, scaled and subtracted to minimize the residuals. An IDL custom-made tool was used to rapidly converge on an acceptable shift and scaling solution. Alternatively, a residual minimization using the AMOEBA[2] function was applied giving consistent results. Figure 1 shows the result of the single image-subtraction image of LkCa15 at a rotator position of 33° corresponding to the set that provides the best contrast. Additionally, we took advantage of the observations taken at two rotator positions to explore dead zones hidden by the secondary spikes and the coronagraphic mask transition (see zoom-i, in Fig. 1). Derotation was also applied to average the speckle patterns and increase the final signal-to-noise. Finally, Double subtraction of images at 0 and 33° were obtained to remove the non-rotating aberrations (related to static optics in NACO) and possibly reveal a positive-negative signature expected for a true companion (and not for instrumental residuals). All sets of single, double-subtracted and derotated-averaged images were finally compared to derive a final subtracted image, optimized at different angular separations.

[1] http://www.eso.org/projects/aot/eclipse/

[2] http://www.physics.nyu.edu/grierlab/idl_html_help/A8.htmlwp992475

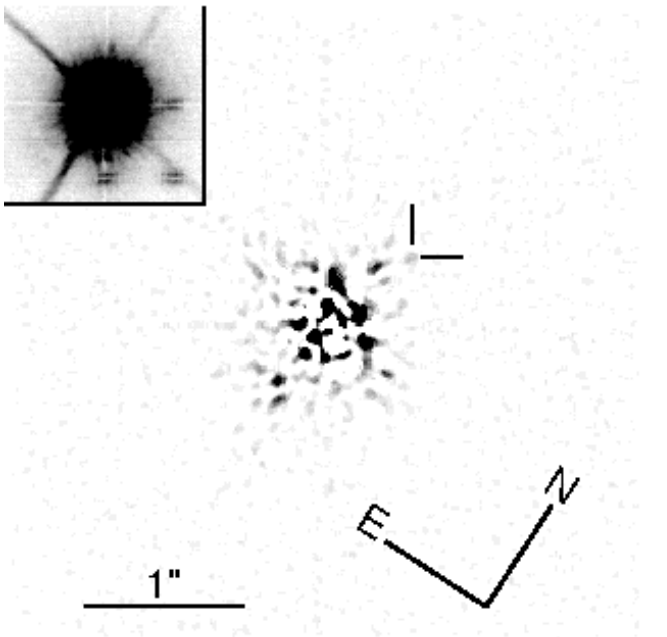

Fig. 1. LkCa15 4QPM coronagraphic image at a rotator position of 33° after PSF subtraction and spatial filtering. The zoom-in non-subtracted image is reported on the *upper-left corner* with the same field of view and thresholds.

4.3. Detection limit

Using our final residual image, a pixel-to-pixel 2D noise map was estimated using a sliding box of 5×5 pixels over the whole NACO FoV (see Fig. 2 and 1D-detection limits in Fig. 3). The 6σ detection limit map was obtained after renormalization by the LkCa15 images obtained in classical imaging and applying all corrections related to the use of different optical set-ups: exposure times (see Table 1), neutral density and Lyot-stop transmissions (a factor of 1.12% and 80.8% respectively, according to Boccaletti et al. 2008) and $NB_{2.17}$ to K_s filter transformation. Finally, we also took into account that the four-quadrant mask causes an attenuation of the off-axis objects due to the 4QPM transition, decreasing our sensitivity close to the axis (see Boccaletti et al. 2004). Compared to previous deep imaging surveys with no a-priori information on the orbital configuration of the system, the LkCa 15 disk system properties offer the possibility to set constraints on the orbital properties of a possible co-planar companion. The use of the complete 2D-detection map is therefore mandatory to fully exploit the sky-projected spatial information of the LkCa 15 environment provided by our direct imaging observations.

5. Results

5.1. Null-detection in the central hole

At separations corresponding to the central hole ($\rho < 0.33''$, 46 AU) no evidence of a point-like object was found in any of our image-subtracted sets. The azimuthal averaged contrast places a limit of $\Delta K_s = 7$ mag equivalent to about $12 M_J$ for a hypothetical projected distance of 30 AU. A statistical approach of this detection limit is analyzed thoroughly in Sect. 5.2. We

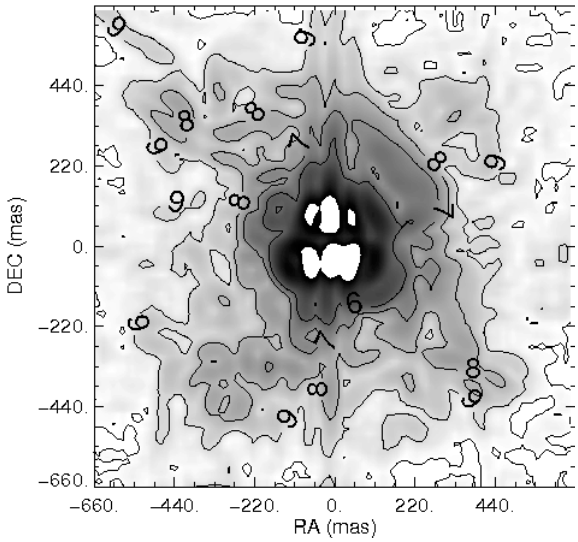

Fig. 2. ΔK_S contrast map giving the contrast between the faintest target detectable at a 6σ level and the primary star.

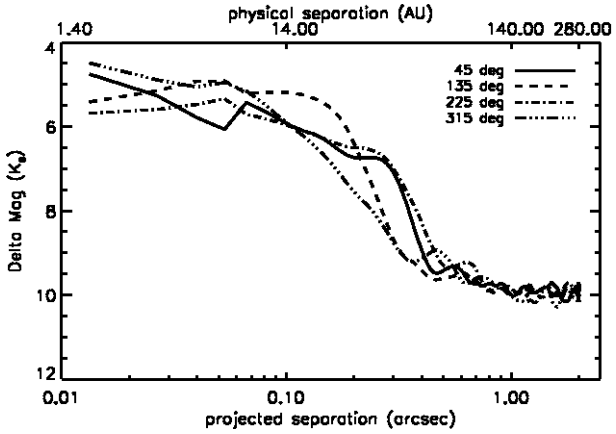

Fig. 3. Four different ΔK_S 1D-contrast detection limits extracted at four position angles (45, 135, 225 and 315 degrees) for comparison. They illustrate the azimuthal variation at close inner angles due to the NACO PSF structure and the importance of using a contrast map to take that effect into account.

also searched for point-like objects at separations that are not compatible with the central hole. We found a low significant point-source at a separation of $\rho = (0.67 \pm 0.02)''$ at a position angle of PA $= (340.7 \pm 0.3)°$. Although close to the detection limit, this point-source lies at the boundary between the speckle and the background noise regimes and is then visible in the subtracted image of Fig. 1. We roughly estimated a contrast of $\Delta K_s = 10.2$ mag in a five pixel aperture. Error bars are not estimated as the point-source is quite close to the noise level (less than 6σ if we refer to Fig. 3), so the previous contrast value should be taken with caution. There are a number of artifacts that may produce such patterns like waffle and spiders. The nearest spider spike, the trace of which is still visible in Fig. 1, is offset by 25° while the waffle mode appears in a 45° direction at a position of 0.49″ and is therefore not compatible with the presence of this point-source. However, it is not visible in the subtracted image obtained for the 0° rotator position, while at this separation the detection limit is almost similar for both rotator positions (see Fig. 2). But the point-source would be at about 0.2″ from the vertical 4QPM transition and slightly attenuated. As it is difficult to rule out a structure in the speckle pattern, additional observations will be mandatory to test this potentially low-mass object.

5.2. Companion mass and orbital parameters

5.2.1. Simulation description

A first step is to convert our 6σ detection limit map in terms of minimum mass map. This is usually done considering the star's apparent magnitude in the K_s-band and its distance, finally the evolutionary model predictions at the age of the system to convert the absolute magnitude limits derived in the NACO filters in masses. We considered here an age of 4 Myr and a distance of 140 pc for LkCa15. We then looked at two classes of evolutionary models based on different assumptions on the initial conditions: hot-start models considering an initial spherical contracting state (Chabrier et al. 2000; Baraffe et al. 2003; Saumon & Marley 2008) and core accretion models coupling planetary thermal evolution to the predicted core mass and thermal structure of a core-accretion planet formation model (Marley et al. 2007; Fortney et al. 2008). In the case of the core-accretion model predictions, our detection performances do not allow to access the planetary mass regime at all. Massive hot Jupiters are indeed predicted to be much fainter at young ages (Marley et al. 2007). Therefore, minimum mass maps were determined using the hot-start model predictions over the planetary and brown dwarf mass-regime.

In a second step we used our minimum mass maps to calculate the detection probability (P_D) of companions of various masses and orbital parameters (semi-major axis a, eccentricities e, inclination i, longitude of the ascending node Ω, longitude of periastron ω and time of periastron passage T_p). With regard to the disk properties (inclination, position angle and inner radius), different assumptions can be made to fix partially the companion orbital properties. The rest of the orbital parameters can be randomly generated. Each simulated companion is then placed on our 2D minimum mass map according to its position on the projected orbit and its detectability is tested, comparing its mass with the minimum value achievable at the same position in the FoV. Running the simulation 10 000 times for a given set of mass and orbital parameters enabled us to derive a detection probability. As already pointed out in Sect. 4.3, we took advantage of both the available information on the disk geometry and the spatial information of the detection limit map, to test all probable sets of physical and orbital parameters for a putative companion.

The smallest projected physical separation probed around LkCa15 is limited by the 4QPM coronagraph attenuation inside 0.15″ (equivalent to three times the angular resolution), setting the minimum semi-major axis considered in our simulations to 20 AU. Projected physical separations as large as 1000 AU were explored, but we decided to restrain our study to the close circumstellar environment considering the semi-major axis $a = [20, 280]$ AU. Additionally, we restrained the parameter space explored for $M = [3, 100]\ M_{Jup}$ and the eccentricity $e = [0., 0.3]$.

5.2.2. Results

In Fig. 4 the results of our simulation are given as a non-detection probability map as a function of the companion mass and semi-major axis. We considered the most constraining case of a coplanar orbit with an inclination and a longitude of the ascending node fixed by the disk properties: $i_{Disk} = 49°$

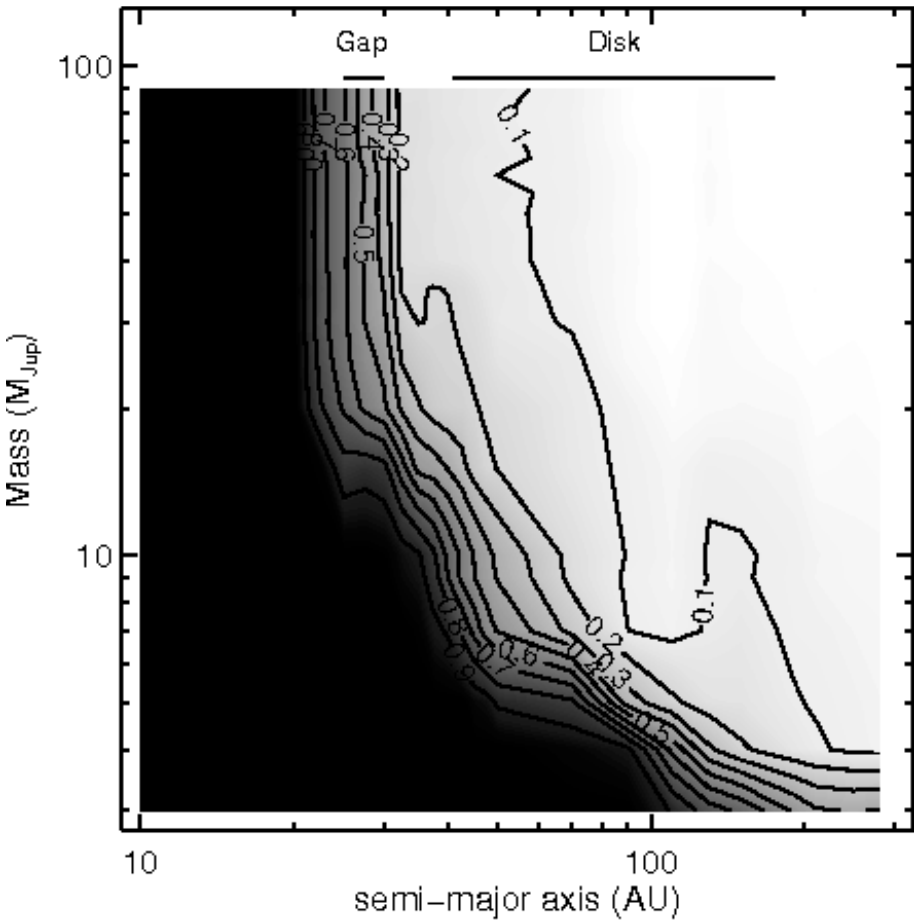

Fig. 4. Non-detection probability map of a faint companion as a function of its mass and semi-major axis in the case of a null-eccentricity (circular) orbit solution. Inclination and longitude of the ascending node have been fixed using the disk properties: $i_{\rm Disk}$ = 49° and Ω = $\rm PA_{Disk}$ ± 90° (= 151 ± 90).

and Ω = $\rm PA_{Disk}$ ± 90° (= 151 ± 90°). Only the null-eccentricity map is show, but the solutions for low-eccentricities (e < 0.3) are not significantly different. The range of the semi-major axis estimated for the predicted candidate companion (25-35 AU, see Piétu et al. 2006) and the disk boundaries (46−177 AU) are reported, as given in Piétu et al. (2007).

Any low stellar-mass companion should have been detected with a high confidence level (non-detection probability lower than 0.1) for a semi-major axis larger than 55 AU (non-detection probability of 0.2 at 30 AU). Any brown dwarf companion with masses larger than 10 $M_{\rm Jup}$ should have been detected for a semi-major axis larger than 80 AU with a non-detection probability of 0.1 (60 AU for 0.2). Our non-detection probability map shows that we start exploring the planetary mass regime, but do not reach deep enough to reject the presence of any massive giant planet at the location of the disk depletion (non-detection probability higher than 0.9 at 20−35 AU). For this physical separation, the presence of more massive companions of 20 $M_{\rm Jup}$ or more cannot be excluded with certainty. At larger distances (a > 100 AU), companions of a mass of more than 6 $M_{\rm Jup}$ seem unlikely. Although we only explored low-eccentricity solutions in a systematic way, the above results also provide lower limits on the detection probabilities for higher eccentricity values, as the time spent far from the star becomes progressively longer.

5.2.3. Limitations

As for all the current deep (or even wide field) imaging studies of young, very low-mass objects or companions (see e.g. Nielsen & Close 2010; Chauvin et al. 2009; Lafrenière et al. 2007; Marois et al. 2008), the main limitations of our analysis come from the conversion of our detection limits in terms of minimum detectable masses. They are related to the uncertainty in the age determination of LkCa15 and the use of non-calibrated evolutionary models for young ages and very low masses. By comparison, uncertainties on the system distance and $K_{\rm s}$ apparent brightness are negligible. Age and model predictions are discussed below.

1. The source LkCa15 is a confirmed member of the Taurus-Auriga association, for which an age of 3−5 Myr is estimated (Simon et al. 2000). To explore how the age uncertainty affects our results, we ran similar simulations for ages of 1, 4 and 7 Myr. The impact of the age uncertainty is much more significant in the planetary mass domain than in the brown dwarf regime. Consequently, it does not significantly affect our conclusions relative to the presence of a brown dwarf or a low-mass stellar companion around LkCa15.
2. The applicability of evolution tracks of brown dwarfs at ages less than a few million years have been already cautioned by Baraffe et al. (2003). The role of the initial conditions has also been questioned by Marley et al. (2007), specifically for young giant planets where a connection between giant-planet formation and evolution models seems mandatory. At the location of the LkCa15 inner disk cavity (between 20 and 46 AU), our 4QPM observations are not sensitive at all to the apparent magnitudes predicted for planetary-mass companions described by the core accretion start models. They are marginally sensitive for high planetary masses with fluxes predicted by the Hot Start models. The strongest constraints are actually set in the brown dwarf regime for masses larger than M ≥ 20 $M_{\rm Jup}$, where the Hot Start evolutionary

models are more appropriate. Although these models still need to be more extensively calibrated for this range of masses and ages, recent discoveries of young calibrators (Mohanty et al. 2004; Close et al. 2005; Stassun et al. 2006) indicate that their predictions are relatively faithful regarding the accuracy required in our study. Our conclusions related to the probable presence of a brown dwarf or low mass star companion responsible for the inner hole detected in the LkCa15 disk remain then meaningful down to 30 AU.

6. Conclusions

The T-Tauri star LkCa 15 was observed with VLT/NACO using the 4QPM coronagraph, reaching a contrast of less than 9.5 in K_s band at separations higher than 0.5″. Our goal was the detection of a low-mass companion, with a mass spanning from 0.2 $M_\odot$ down to 5 $M_{\rm Jup}$, whose presence has been suggested as an explanation for the large cavity shown by sub-millimeter observations in the disk surrounding the star.

We do not report any positive detection of a close companion of the star LkCa15. Based on our detection limits and Hot Start evolutionary model predictions, we ran simulations to take into account a putative companion should enable us to constrain its mass and semi-major axis given reasonable assumptions from the disk geometry.

The innovative approach in our case is the combined use of both the available information about the disk configuration (inclination, ascending node, gap prediction) and the complete 2D information of the coronagraphic image to actually constrain the probability of existence of a stellar or sub-stellar companion around LkCa15. As a main result of our statistical analysis we can exclude a low-mass star and brown dwarf companion with a semi-major axis larger than 55 and 80 AU respectively. The planetary-mass regime is only partially constrained and at a large semi-major axis ($a \geq 100$ AU) huge ($M \geq 6\ M_{\rm Jup}$) planetary-mass companions seem unlikely.

The limitations of our study are also discussed with regard to the LkCa15 age-uncertainty that does not much affect our conclusions for low-mass stars and brown dwarf companions, and with regard to the uncertainty related to the initial conditions adopted for the evolutionary model, which are particularly critical in the planetary mass regime. Finally, for a true companion orbiting LkCa15 in the inner disk cavity, our observations would favor a planetary-mass or low-mass brown dwarf companion, although more massive companions cannot be completely excluded with high detection probability.

Further deep imaging studies at the 5−50 AU scale at a new epoch should provide complementary information to completely reject the existence of a close stellar or brown dwarf companion of LkCa15 and pursue the search for the putative companion that would be responsible for the disk geometry and inner cavity within 46 AU.

References

Alexander, R. D., Clarke, C. J., & Pringle, J. E. 2006, MNRAS, 369, 229
Augereau, J. C., Lagrange, A. M., Mouillet, D., & Ménard, F. 1999, A&A, 350, L51
Baraffe, I., Chabrier, G., Barman, T. S., Allard, F., & Hauschildt, P. H. 2003, A&A, 402, 701
Bergin, E., Calvet, N., Sitko, M. L., et al. 2004, ApJ, 614, L133
Bertout, C., & Genova, F. 2006, A&A, 460, 499
Bertout, C., Siess, L., & Cabrit, S. 2007, A&A, 473, L21
Boccaletti, A., Riaud, P., Baudoz, P., et al. 2004, PASP, 116, 1061
Boccaletti, A., Chauvin, G., Baudoz, P., & Beuzit, J.-L. 2008, A&A, 482, 939
Chabrier, G., Baraffe, I., Allard, F., & Hauschildt, P. 2000, ApJ, 542, 464
Chauvin, G., Lagrange, A.-M., Bonavita, M., et al. 2010, A&A, 509, A52
Close, L. M., Lenzen, R., Guirado, J. C., et al. 2005, Nature, 433, 286
Devillard, N. 1997, The Messenger, 87, 19
Espaillat, C., Calvet, N., D'Alessio, P., et al. 2007, ApJ, 670, L135
Fortney, J. J., Marley, M. S., Saumon, D., & Lodders, K. 2008, ApJ, 683, 1104
Huélamo, N., Figueira, P., Bonfils, X., et al. 2008, A&A, 489, L9
Hughes, A. M., Wilner, D. J., Calvet, N., et al. 2007, ApJ, 664, 536
Kalas, P., Graham, J. R., Chiang, E., et al. 2008, Science, 322, 1345
Lafrenière, D., Doyon, R., Marois, C., et al. 2007, ApJ, 670, 1367
Lenzen, R., Hartung, M., Brandner, W., et al. 2003, in SPIE Conf. Ser. 4841, ed. M. Iye, & A. F. M. Moorwood, 944
Marley, M. S., Fortney, J. J., Hubickyj, O., Bodenheimer, P., & Lissauer, J. J. 2007, ApJ, 655, 541
Marois, C., Macintosh, B., Barman, T., et al. 2008, Science, 322, 1348
Marois, C., Macintosh, B., Barman, T., et al. 2009, in Am. Astron. Soc. Meet. Abstracts, 213, 319.07
Mayor, M., & Queloz, D. 1995, Nature, 378, 355
Mohanty, S., Jayawardhana, R., Natta, A., et al. 2004, ApJ, 609, L33
Nielsen, E. L., & Close, L. M. 2010, ApJ, 717, 878
Piétu, V., Guilloteau, S., & Dutrey, A. 2005, A&A, 443, 945
Piétu, V., Dutrey, A., Guilloteau, S., Chapillon, E., & Pety, J. 2006, A&A, 460, L43
Piétu, V., Dutrey, A., & Guilloteau, S. 2007, A&A, 467, 163
Rousset, G., Lacombe, F., Puget, P., et al. 2003, in SPIE Conf. Ser. 4839, ed. P. L. Wizinowich, & D. Bonaccini, 140
Saumon, D., & Marley, M. S. 2008, ApJ, 689, 1327
Setiawan, J., Henning, T., Launhardt, R., et al. 2008, Nature, 451, 38
Simon, M., Dutrey, A., & Guilloteau, S. 2000, ApJ, 545, 1034
Stassun, K. G., James, D. J., Montalban, J., & Jeffries, R. 2006, in NOAO Proposal ID #2006B-0099, 99